Int. J. Heat Mass Transfer. Vol. 34, No. 11, pp. 2727–2738, 1991
Printed in Great Britain

0017–9310/91 $3.00 + 0.00

Particulate fouling of water in tubes having a two-dimensional roughness geometry

NAE-HYUN KIM
Department of Mechanical Engineering, Kum-Oh National Institute of Technology, Kumi City, Korea

and

RALPH L. WEBB
Department of Mechanical Engineering, The Pennsylvania State University, University Park, PA 16801, U.S.A.

(*Received* 17 *July* 1990 *and in final form* 4 *December* 1990)

Abstract—In this study, a rationally based fouling model is developed. The model, with experimentally determined sticking probability and deposit bond strength factor, can predict the fouling behavior of repeated rib tubes. The mass transfer rate is assumed to control the particle transport process, and the wall shear stress is assumed to control the removal process. The mass transfer rate for repeated rib tubes is obtained from the corresponding heat transfer correlations. The wall shear stress is modeled based on the flow structure between the ribs. Particulate fouling tests are conducted in water. The range of variables investigated in this study are the roughness variables ($0.015 \leqslant e/D \leqslant 0.030$ and $10 \leqslant p/e \leqslant 20$). Reynolds number ($14\,000 \leqslant Re \leqslant 26\,000$) and the foulant material (ferric oxide and aluminum oxide). The tube material is copper, and the rib cross-section is arc-shaped. Empirical correlations define the effect of the geometric and flow parameters on the sticking probability and bond strength factor. An analysis is performed that accounts for the forces acting on the particles at the wall. The analysis suggests that the hydrodynamic force is dominant for the present tests. This analysis qualitatively supports the empirically obtained geometric and Reynolds number dependencies of the sticking probability.

1. INTRODUCTION

FOULING can be defined as the accumulation of undesired deposits on heat transfer surfaces. This accumulation of deposits adversely affects the thermal and hydraulic performance of the surfaces, and thus increases both the initial and operating costs of a heat exchanger. When fouling occurs by the accumulation of fine particles suspended in the process fluid, it is categorized as 'particulate fouling'. In this study, discussions will be limited to particulate fouling.

Enhanced tubes have been widely used because of their superior heat transfer performance. The inside geometries are usually helical-rib, three-dimensional (3-D) roughness or corrugated. The effect of fouling on enhanced tubes could be worse than that on smooth tubes because it may degrade the superior heat transfer performance by filling the gap of the roughness elements with foulants. The literature contains very little data on fouling in enhanced tubes. The few investigations that have been carried out address particulate and precipitation fouling. The particulate fouling behavior of commercial enhanced tubes was investigated in ref. [1] and the results were compared with that of a smooth tube. It was shown that the enhanced tubes fouled almost the same as that of the smooth tube at $Re \approx 30\,000$. At lower Reynolds numbers, however, the enhanced tubes showed higher fouling resistance. Ferric oxide and aluminum oxide were used as the foulants, and the concentration was 1500 ppm. Patun *et al.* [2] performed particulate fouling tests on spirally-ribbed tubes. However, no comparison with plain tube fouling is given. Watkinson *et al.* [3] conducted scaling experiments on spirally indented tubes, and found that the fouling resistances were essentially the same as those of a plain tube. Dreytser *et al.* [4] performed scaling tests inside tubes having ring-type turbulence promoters, and found that the fouling resistance is smaller than in plain tubes. Several experimental data are also available for the fouling of externally finned tubes [5–7].

This study is concerned with the particulate fouling of tubes having two-dimensional repeated-rib roughness. Figure 1 shows a tube with repeated rib roughness. The roughness is described by its dimensionless height e/D, dimensionless width w/e and its dimensionless spacing p/e. The objectives of this study are to develop a fouling model which can be applied to repeated rib tubes and to investigate the fouling behavior of repeated rib roughened tubes using the proposed model.

Particulate fouling results from the combined effect of the deposition and removal process. The deposition process may be divided into the transport of particles to the wall and the adhesion of particles at the wall. The net deposition rate $\dot{m}_f$ may be written as

NOMENCLATURE

A_i tube inside area, πDL [m^2]
$B(e^+)$ friction roughness function [dimensionless]
C_b concentration at the bulk stream [kg m^{-3}]
C_p specific heat [J kg^{-1} K^{-1}]
D tube inside diameter [m]
d_p diameter of the particle [m]
d_p^+ non-dimensional particle diameter, $d_p u^*/\nu$ [dimensionless]
e height of the rib [m]
e^+ roughness Reynolds number, $e/D\sqrt{(f/2)}Re$ [dimensionless]
f friction factor [dimensionless]
F_i interaction force between a particle and the deposit [N]
F_L hydrodynamic lift force acting on a particle at the deposit surface [N]
F_{net} net force acting on the particle at the deposit surface [N]
$g(e^+)$ heat transfer roughness function [dimensionless]
h height of the deposit surface micro-roughness [m]
H particle separation distance [m]
k_f thermal conductivity of the deposit [W m^{-1} K^{-1}]
K_m mass transfer coefficient [m s^{-1}]
L length of the test section [m]
$LMTD$ log mean temperature difference [K]
m_f deposit mass per unit surface area [kg m^{-2}]
$\dot{m}_f$ net deposition flux [kg m^{-2} s^{-1}]
$\dot{m}_w$ water flow rate [kg s^{-1}]
p pitch of the rib [m]
Pr Prandtl number [dimensionless]
q heat transferred to the test section [J s^{-1}]
R_f fouling resistance [m^2 K W^{-1}]
R_f^* asymptotic fouling resistance [m^2 K W^{-1}]
$\dot{R}_{f0}$ initial fouling rate [m^2 K J^{-1}]
Re Reynolds number, $u_m D/\nu$ [dimensionless]
S sticking probability [dimensionless]
s spacing between the deposit surface micro-roughness [m]
Sc Schmidt number [dimensionless]
St Stanton number [dimensionless]
St_m mass transfer Stanton number [dimensionless]
T_{in} temperature at the inlet of the test section [K]
T_{out} temperature at the exit of the test section [K]
t time [s]
t_c time constant defined by equation (6) [s]
t_p^+ dimensionless particle relaxation time [dimensionless]
U_c overall heat transfer coefficient at a clean condition [W m^{-2} K^{-1}]
U_f overall heat transfer coefficient at a fouled condition [W m^{-2} K^{-1}]
u local flow velocity [m s^{-1}]
u_m mean flow velocity [m s^{-1}]
u^* friction velocity, $\sqrt{(\tau_w \rho)}$ [m s^{-1}]
u^+ non-dimensional velocity, u/u^* [dimensionless]
w width of the rib [m]
x coordinate parallel to the flow direction [m]
y coordinate normal to the flow direction [m]
y^+ non-dimensional distance, yu^*/ν [dimensionless].

Greek symbols
μ absolute viscosity [N s m^{-2}]
ν kinematic viscosity [m^2 s^{-1}]
ξ deposit bond strength factor [N s m^{-2}]
ρ_f density of the deposit [kg m^{-3}]
ρ_p density of the particle [kg m^{-3}]
τ_w wall shear stress [N m^{-2}]
ϕ_d deposition rate [kg m^{-2} s^{-1}]
ϕ_r removal rate [kg m^{-2} s^{-1}].

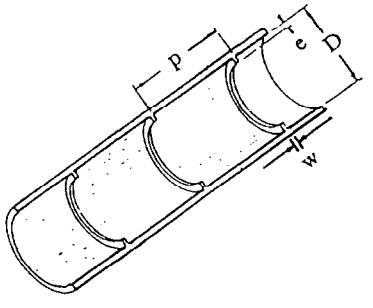

FIG. 1. Sketch of a tube with repeated rib roughness.

$$\dot{m}_f = \phi_d - \phi_r \quad (1)$$

where ϕ_d is the deposition rate and ϕ_r the removal rate. Each term may be written as follows [8]:

$$\phi_d = K_m S C_b \quad (2)$$

$$\phi_r = \frac{m_f \tau_w}{\xi} \quad (3)$$

where S is the sticking probability—a probability that a transported particle will stick to the wall—and ξ the deposit bond strength factor. In equations (2) and (3),

K_m is the mass transfer coefficient and τ_w the wall shear stress.

Insertion of equations (2) and (3) into equation (1) yields the following asymptotic fouling resistance equation:

$$R_f = R_f^*(1-e^{-t/t_c}) \tag{4}$$

where

$$R_f^* = \frac{\phi_d t_c}{\rho_f k_f} \tag{5}$$

and

$$t_c = \frac{\xi}{\tau_w}. \tag{6}$$

Equations (5) and (6) show that fouling behavior can be predicted if the mass transfer coefficient K_m, the wall shear stress τ_w, the sticking probability S, and the bond strength factor ξ are known (assuming that we know the deposit density ρ_f and the deposit thermal conductivity k_f). In this study, K_m and τ_w will be modeled for repeated rib tubes, and S and ξ will be evaluated from experimental results.

2. FOULING MODEL FOR REPEATED RIB TUBES

2.1. *Formulation of mass transfer coefficient* K_m

Experimental data on the particle deposition suggests three distinct regimes: diffusion, inertia and impaction [9]. In the diffusion regime ($t_p^+ < 0.2$), Brownian motion controls the deposition, and thus the fine particle transport rate may be obtained from the traditional mass transfer correlation. In the inertia regime ($0.2 < t_p^+ < 10$), the particles are rather large that turbulent eddies give the particles a radial velocity to penetrate the viscous sublayer. In the impaction regime ($t_p^+ > 10$), the particles are sufficiently large that the deposition velocity becomes of the order of the friction velocity (u^*). t_p^+ is a dimensionless particle relaxation time, which is defined as follows:

$$t_p^+ = \frac{\rho_p d_p^2 (u^*)^2}{18\mu\nu}. \tag{7}$$

Equation (7) shows that t_p^+ increases as the particle diameter (d_p) or Re increases. For the case of a ferric oxide–water suspension flowing at $Re = 30\,000$ inside the tube with i.d. = 15.2 mm, the diffusion regime extends up to $d_p = 10$ μm. Thus, this regime is probably the most important regime in industrial applications. In this study, discussions will be limited to the diffusion regime.

In the diffusion regime, K_m may be obtained from a heat transfer correlation based on the heat–mass transfer analogy. It is well known that the heat transfer from rough surfaces can be predicted from the following equation [10]:

$$St = \frac{f/2}{1+\sqrt{(f/2)}[g(e^+)Pr^n - B(e^+)]} \tag{8}$$

where $B(e^+)$ and $g(e^+)$ are friction and heat transfer roughness functions, respectively. Those roughness functions may be obtained from friction and heat transfer tests. Making use of the analogy between heat and mass transfer, equation (8) may be used to predict the mass transfer rate if St and Pr are replaced by St_m and Sc, respectively. Equation (8) was originally developed for the heat transfer on repeated rib tubes where Pr was varied between 0.7 and 38. For the case of fine particle transport, Sc is of the order of 10^5–10^6. Thus, one should be cautious of directly applying equation (8) to determine the fine particle transport rate. Hahn *et al.* [11] investigated the fine particle transport on repeated rib roughness with the p/e range of 2–25. They successfully correlated their data with the Kader and Yaglom [12] correlation, which was originally developed for the heat and mass transfer on repeated rib geometries. This suggests that the conventional rough surface heat transfer correlation (equation (8)) may be used to predict the fine particle transport rate. For the high Sc range, equation (8) can be simplified to the following form:

$$St_m = \frac{K_m}{u_m} = \frac{\sqrt{(f/2)}}{g(e^+)Sc^n}. \tag{9}$$

For repeated rib tubes, excellent correlations for $g(e^+)$ were found [13]. They are

$$g(e^+) = 8.5(e^+)^{0.1} \quad \text{for} \quad 10 < e^+ < 20 \tag{10}$$

$$g(e^+) = 4.75(e^+)^{0.28} \quad \text{for} \quad e^+ > 26 \tag{11}$$

where $e^+ = e/D\sqrt{(f/2)}Re$ and may be obtained from the friction test. It was also found that the Schmidt number exponent $n = 0.57$ correlated the data [13].

2.2. *Modeling of the wall shear stress* τ_w

For a smooth tube, wall shear stress is the only component which contributes to friction. For rough surfaces however, a substantial fraction of the pressure drop may be due to profile drag on the roughness elements. In this study, it is assumed that the profile drag does not contribute to the removal process. Only pure wall shear stress is assumed to contribute to the removal of particles from the wall. Thus, it is necessary to quantify the wall shear stress between the rib elements.

Based on the flow structure between ribs [14], a four region model is proposed (Fig. 2). Region 1 is a forward flow region on top of the rib, region 2 is a recirculating region behind the rib, region 4 is a recirculation region in front of the rib, and region 3 is a forward flow region between regions 2 and 4. Then, the wall shear stress τ_w may be obtained from the following relations:

$$A_w\tau_w = A_1\tau_1 + A_2\tau_2 + A_3\tau_3 + A_4\tau_4. \tag{12}$$

Lewis [15] proposed an elementary model which can predict the apparent wall shear stress. In the development of his model, Lewis assumed that the turbulent sublayer thickness over a rough surface is decreased because of the increase in local turbulence

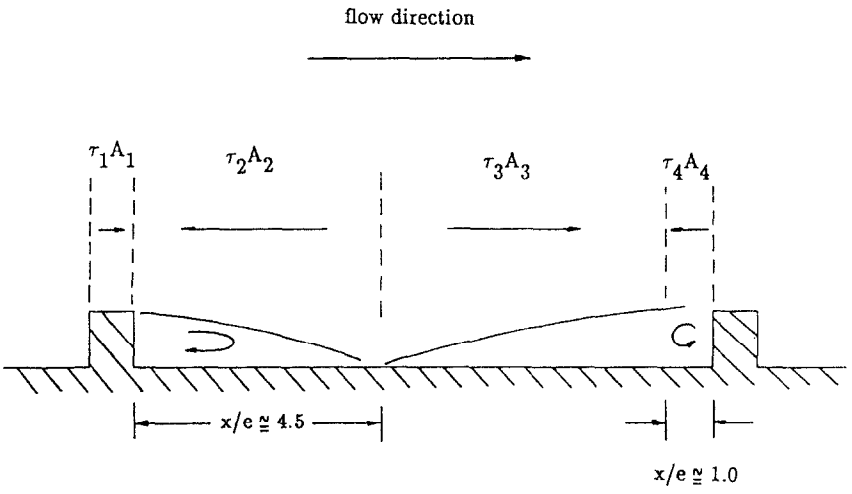

FIG. 2. Proposed wall shear stress model.

intensity generated by separated flow. Applying this idea to the forward flow zone (regions 1 and 3 in Fig. 2), he successfully predicted the apparent wall shear stress of the repeated rib tubes. In the development of his model, however, he assumed that the negative wall shear stress in the recirculating flow regions (regions 2 and 4) is included in the form drag.

In this study, τ_1 and τ_3 are calculated from Lewis's model, and τ_2 and τ_4 are obtained from the measurements by Lavallee and Popovich [14], which show approximately the same magnitude of wall shear stress both in the forward and recirculating regions. The wall shear stress in the recirculating zone may be a function of Reynolds number and e/D. However, it is not likely to be a function of p/e. Thus, in this study, the wall shear stress in the recirculating zone is obtained from Lavallee and Popovich's measurement, and is assumed to be independent of p/e.

Table 1 shows Lavallee and Popovich's measurement ($p/e = 12.52$, $e/D = 0.05$) compared with the prediction from this study. The table shows that the current model predicts the wall shear stress reasonably well, considering the possible error involved in the wall shear stress measurement.

2.3. *Sticking probability S and deposit bond strength factor* ξ

Consider the particles transported to the wall. They will start to adhere at the bare tube wall. Once the tube wall is fully covered with particles, the particles will adhere to the pre-deposited particles. For a precise analysis, the adhesion process should be analyzed considering two steps—particle–wall interaction and particle–deposit interaction. It was estimated that the deposit thickness which yields moderate thermal fouling resistance is of the order of 100 μm [16]. If we assume that the particle diameter is 1 μm, the deposit layer will be of the order of a hundred fold. Thus, in this study, the particle–wall interaction is neglected, and only particle–deposit interaction is considered.

Table 1. Comparison between the measured and predicted wall shear stress

Re	Lavallee and Popovich [14]	Prediction (this study)
8580	5 (g cm^{-1} s^{-2})	8
21 700	36	45

The adhesion and removal term may be understood by study of the basic interaction forces between particles and the deposit. Three important forces—London–Van der Waals force, electric double layer force and hydrodynamic lift force may be identified. The London–Van der Waals force and the electric double layer force have been studied by several investigators [17, 18]. On the contrary, the fluid dynamic force—a force acting on transported particles at the wall location—has not been discussed in the referenced publications, and thus will be discussed here.

Velocity measurement of turbulent flow inside a tube shows a viscous sublayer near the wall. For the 2 μm ferric oxide depositing on a tube wall flowing at $Re = 30\,000$ inside the tube with i.d. = 15.2 mm, $d_p^+ \approx 0.2$. Then, the particle is fully submerged in the viscous sublayer ($y^+ \leqslant 5$). In this region, the velocity profile is linear and may be written as

$$u^+ = y^+. \tag{13}$$

Figure 3 shows a particle depositing on the deposit surface which is assumed to have a micro-roughness (height h, spacing s). Two different cases of the particle–deposit interaction are shown. In case 1, the particle separation distance H is rather large compared with that in case 2. In the figure, F_L is the hydraulic lift force and F_i the interaction force which is obtained by adding the electric double layer force and the Van der Waals force.

Then, the net adhesive force acting on the particle may be written as

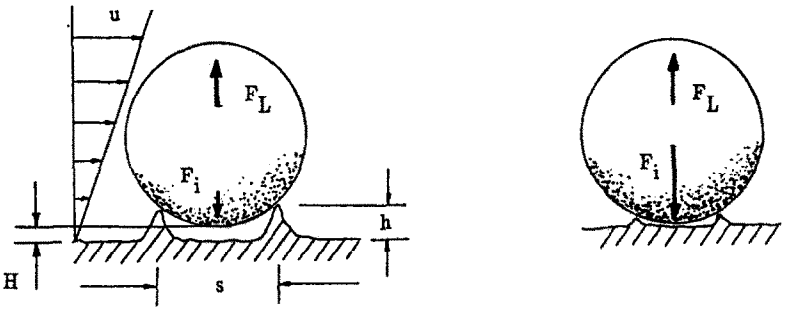

FIG. 3. Forces acting on a particle at the wall.

$$F_{net} = F_i - F_L. \quad (14)$$

The hydraulic lift force was given by Hubbe [19] as

$$F_L = \frac{11.0 d_p^3 \tau_w}{s}. \quad (15)$$

Detailed information on F_i is given by Visser [17]. If F_i is smaller than F_L (case 1 in Fig. 3) the particle may roll over the wall, and eventually adhere at a place where F_i is larger than F_L (case 2 in Fig. 3).

In this study, ferric oxide and aluminum oxide particles were used as foulants. The suspending liquid was city water with pH = 8.0. Table 2 shows the values of four important parameters used to determine the interaction forces. The Hamaker constant determines the strength of the Van der Waals force, and the zeta potential determines the strength of the electric double layer force. The foulant sample was obtained during the test, and the particle size was measured using a particle size analyzer (HORIBA model CAPA 500). The zeta potential was measured using an electrophoretic potential meter (Pen Kem Inc., Model 501 Laser Zee Meter). Table 2 shows that the particle characteristics are similar for both materials. Thus, we may anticipate that the fouling behavior of both materials are similar.

Using this information, F_{net} was calculated by equation (14) for a ferric oxide suspension (pH = 8.0 and $s = 71$ nm), and the results are shown in Fig. 4. The particle shape was assumed to be spherical, and the value of s (deposit surface micro-roughness spacing) was adopted from Hubbe [19]. Figure 4 shows that F_i becomes negligible if the particle separation distance becomes larger than 1 nm. In that case, the hydrodynamic force controls the adhesion process. The detailed calculation procedure is given in ref. [16].

Table 2. Foulant characteristics

	Ferric oxide	Aluminum oxide
Particle diameter (μm)	2.11	1.75
Particle density (kg m^{-3})	5240	3970
Hamaker constant (J)	3.4×10^{-20}	4.2×10^{-20}
Zeta potential (mV)	−13	−14

In this study, the sticking probability and the bond strength factor will be deduced from the experimental data, and the trends will be compared with those from previous analysis. The procedure is as follows:

(1) Curve-fit the fouling data to the asymptotic form

$$R_f = R_f^*(1 - e^{-t/t_c}) \quad (16)$$

$$\dot{R}_{f0} = R_f^*/t_c. \quad (17)$$

(2) Calculate the sticking probability from the initial fouling rate

$$S = \dot{R}_{f0} \frac{\rho_f k_f}{K_m C_b}. \quad (18)$$

(3) Calculate the bond strength factor from R_f^* and $\dot{R}_{f0}$

$$\xi = \tau_w \frac{R_f^*}{\dot{R}_{f0}}. \quad (19)$$

3. RESULTS AND DISCUSSION

3.1. *Brief description of the fouling apparatus*

Figure 5 shows a schematic drawing of the apparatus. The apparatus is capable of testing four tubes simultaneously. Heat is transferred to the 3.05 m long test section by condensing R-114 on the annulus side of the test section. The temperatures are measured using thermistors and the condensing pressures are measured using pressure transducers. The instrumentation capabilities provide a maximum resolution error of 13% in measurement of the fouling resistance. This is the minimum ability of the instrumentation to sense the change in the fouling resistance. The error could be larger at the initial stage of fouling, when the temperature change by fouling is small. A detailed description of the fouling apparatus is provided in ref. [16].

Three repeated rib tubes and a smooth tube were tested. The roughness dimensions are provided in

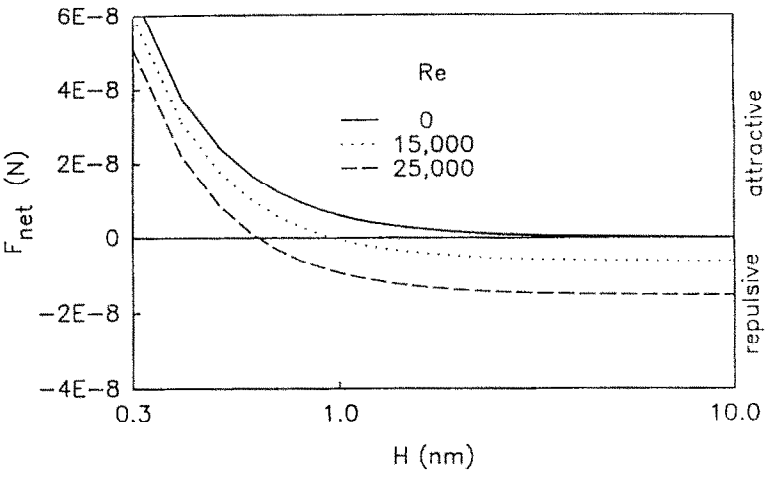

FIG. 4. Net force (F_{net}) vs particle separation distance (H).

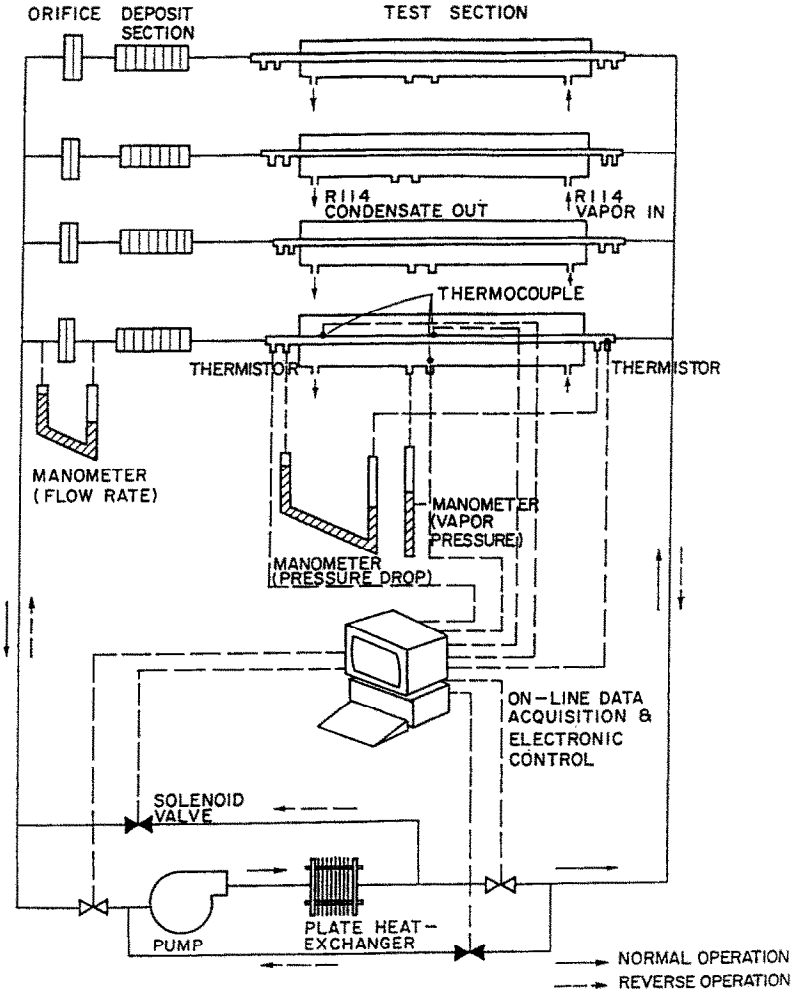

FIG. 5. Schematic drawing of the fouling apparatus.

Table 3. Roughness dimensions of the tubes

Tube	i.d.	e/D	p/e	w/e
30/20	17.0	0.030	20	3.0
30/10	17.0	0.030	10	3.0
15/10	17.0	0.015	10	4.6
Smooth	14.1			

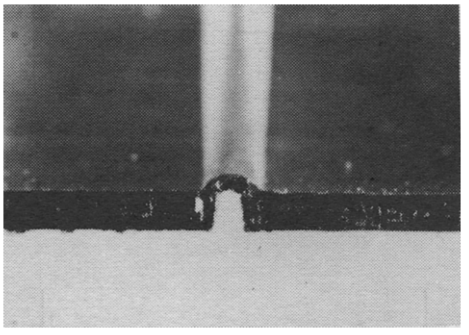

FIG. 6. Photograph of the rib cross-section.

Table 3. The tube inside diameter D is defined as the diameter to the base of the repeated ribs. The repeated rib tubes were made from hard drawn smooth copper tubes. The ribs were made manually by applying a localized pressure on the outer surface of the tube. A tube cutter with a dull edge was used to form the roughness. As a consequence, the cross-section of the rib was arc-shaped. Figure 6 shows a photograph of the rib cross-section. The smooth tube has a smooth inner surface with 14.1 mm i.d. and integral fins (1024 fins m^{-1}, 1.5 mm fin height) on the outer surface.

3.2. *Data reduction*

The fouling resistance is calculated as follows. First, the overall heat transfer coefficient (U_c) based on the inside surface area (A_i) is measured for the clean tube-side condition. Then, the overall heat transfer coefficient is measured for the fouled condition (U_f). The fouling resistance R_f is obtained by

$$R_f = \frac{1}{U_f} - \frac{1}{U_c} \tag{20}$$

where

$$U = \frac{q}{A_i(LMTD)} \tag{21}$$

$$q = \dot{m}_w c_p (T_{out} - T_{in}). \tag{22}$$

In equation (20), it is implicitly assumed that the tube-side heat-transfer coefficient remains constant during the fouling test. The effect of the deposit on tube-side heat transfer performance was estimated in ref. [16], and it was concluded that it is negligible in this test range.

3.3. *Fouling results*

The proposed fouling model, equation (16), requires a knowledge of the sticking probability S and the bond strength factor ζ to predict the fouling behavior. The sticking probability and the bond strength factor may be obtained from the experimental results using equations (18) and (19). K_m was calculated using equation (9) with $g(e^+)$ from equations (10) and (11). Equations (9)–(11) require e^+ as a function of Reynolds number, which were obtained from friction tests. The friction tests were performed at the room temperature (20°C) using water. Figure 7 shows e^+ plotted against Reynolds number.

The wall shear stress was predicted based on the previously described model (equation (12)). Figure 8 shows the predicted wall shear stress plotted against Reynolds number. The figure shows that the wall shear stress increases as e/D increases and p/e decreases.

Fouling tests were conducted at three different Reynolds numbers; Re = 14 000, 19 000 and 26 000. These Reynolds numbers are approximate Reynolds numbers. The exact Reynolds number for each test is shown in Tables 4 and 5. The Reynolds number range may also be presented by the non-dimensional particle relaxation time t_p^+. The range was $0.003 < t_p^+ < 0.02$ (in the diffusion regime). During the test, the inlet water temperature was maintained at 24°C, and the concentration was set at 1500 ppm. The heat flux to the tubes was approximately 13 kW m^{-2}. The average tube wall temperature was between 26 and 28°C.

Figure 9 shows the fouling curves at Re = 14 000 for aluminum oxide. Figure 10 shows the fouling curves at Re = 14 000 for ferric oxide. The shape of curves show asymptotic behavior. The figures clearly show the effect of the roughness configuration. The repeated rib tubes show higher fouling resistances than the smooth tube. Figure 11 shows the fouling curves at Re = 26 000 for aluminum oxide. The fouling resistances of the repeated rib tubes are approximately the same as that of the smooth tube at Re = 26 000. The aluminum oxide fouling curves showed similar behavior [20].

The asymptotic fouling resistances and the initial fouling rates were calculated by curve-fitting the data to the form of equations (16) and (17). S and ξ were calculated from equations (18) and (19). The ferric oxide fouling results are summarized in Table 4, and the aluminum oxide fouling results are summarized in Table 5. The mean flow velocity u_m at the corresponding Reynolds number is also listed in the tables. At the same Reynolds number, the u_m of the smooth tube is about 20% higher than those of the repeated rib tubes because tube inside diameters are different (17.0 mm for the repeated rib tube and 14.1 mm for the smooth tube). Figure 12 shows R_f^* plotted against Reynolds number for aluminum oxide. At Re = 14 000, the repeated rib tubes show much higher R_f^* than the smooth tube. At Re = 26 000, however, they are approximately the same. The R_f^* values for the aluminum oxide were correlated using Re, e/D and p/e as functional groups. The result is

$$R_f^* \propto (e/D)^{-0.3}(p/e)^{0.3}(Re)^{-3.9}. \tag{23}$$

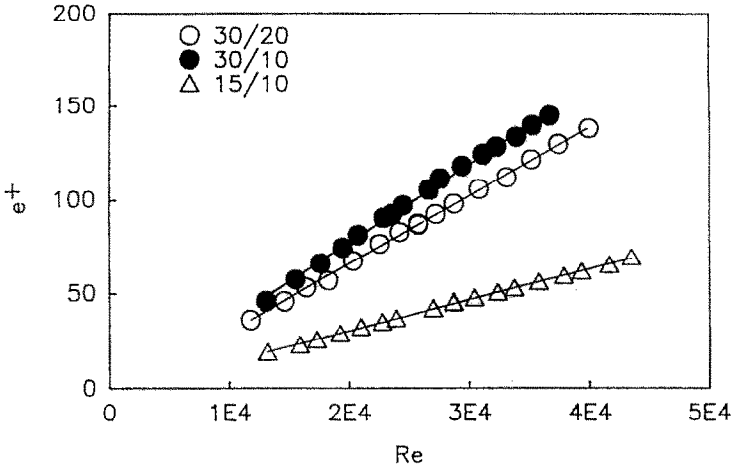

FIG. 7. e^+ vs Reynolds number.

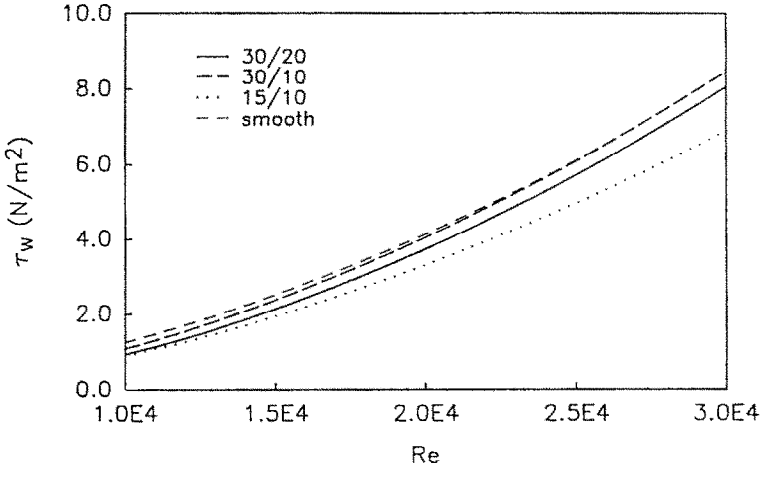

FIG. 8. Predicted wall shear stress vs Reynolds number.

The sticking probabilities and the bond strength factors were also calculated from equations (18) and (19). Tables 4 and 5 show that the bond strength factors are maximum at $Re = 19000$, and show smaller values at $Re = 14000$ and 26000 for all the tubes tested. Thus, no attempt was made to get the Reynolds number exponents of the bond strength factor. The values of the exponents are summarized in Table 6 for both foulants. In the table, F.O. denotes ferric oxide and A.O. aluminum oxide.

Table 4. Ferric oxide fouling results

Tube	Re	u_m (m s^{-1})	R_f^* ($\times 10^6$) (m^2 K W^{-1})	$\dot{R}_{f0}$ ($\times 10^{10}$) (m^2 K J^{-1})	S_{rep}/S_{sm}	ξ ($\times 10^{-4}$) (N s m^{-2})
30/20	13800	0.80	48.1	34.4	1.05	4.36
30/20	18900	1.10	25.9	21.7	0.53	6.59
30/20	25900	1.50	4.8	15.5	0.30	3.02
30/10	14200	0.82	41.0	29.7	0.77	4.97
30/10	18700	1.08	17.4	15.5	0.34	6.67
30/10	25600	1.48	6.5	10.7	0.18	6.48
15/10	14300	0.83	90.3	41.4	1.14	6.05
15/10	19200	1.11	35.5	17.1	0.37	10.0
15/10	25800	1.50	4.1	12.4	0.21	2.77
Smooth	14400	1.00	12.6	5.3	1.00	8.42
Smooth	18600	1.30	10.1	4.8	0.69	11.2
Smooth	26100	1.82	3.1	3.6	0.40	8.50

Table 5. Aluminum oxide fouling results

Tube	Re	u_m (m s^{-1})	R_f^* ($\times 10^6$) (m^2 K W^{-1})	$\dot{R}_{f0}$ ($\times 10^{10}$) (m^2 K J^{-1})	S_{rep}/S_{sm}	ξ ($\times 10^{-4}$) (N s m^{-2})
30/20	13700	0.79	73.0	38.3	0.75	5.51
30/20	18500	1.07	58.1	15.7	0.24	19.0
30/20	25500	1.50	7.8	11.1	0.13	6.73
30/10	14000	0.81	66.4	25.3	0.44	8.35
30/10	18600	1.08	59.8	15.1	0.21	21.8
30/10	25700	1.49	4.9	11.3	0.13	4.07
15/10	14500	0.84	98.2	31.4	0.53	8.35
15/10	18500	1.07	52.8	19.4	0.26	12.4
15/10	25900	1.50	7.2	13.3	0.14	4.39
Smooth	13900	0.97	26.4	8.8	1.00	10.2
Smooth	19500	1.35	23.1	8.1	0.71	15.6
Smooth	26200	1.82	4.8	7.0	0.47	6.62

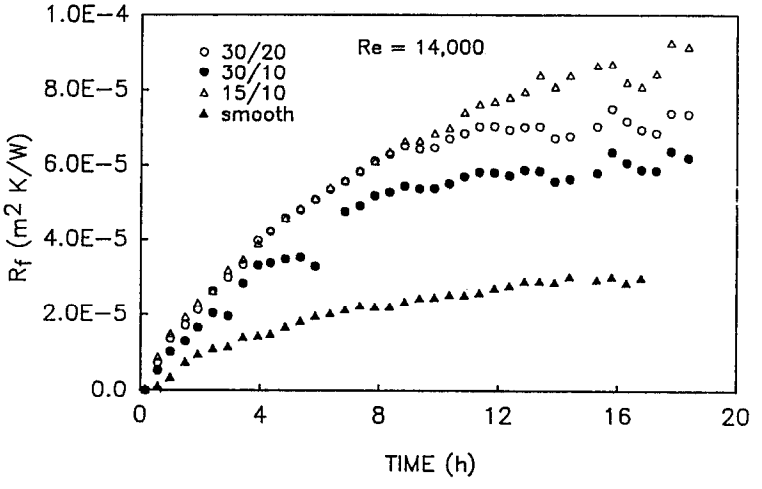

FIG. 9. Aluminum oxide fouling curve, Re = 14000, 1500 ppm.

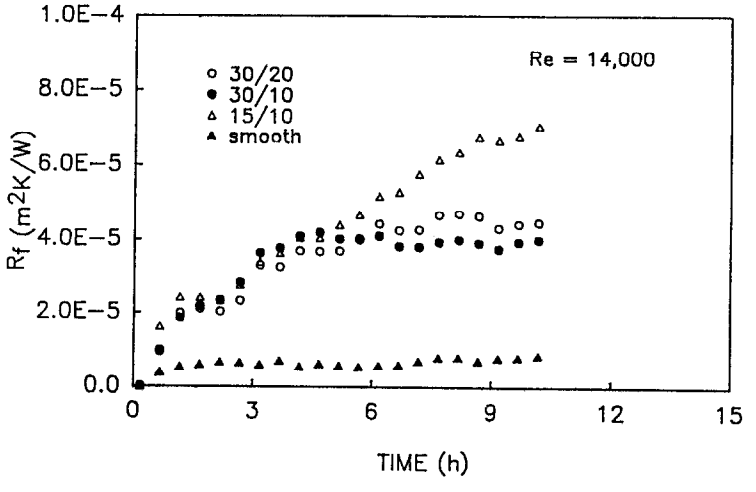

FIG. 10. Ferric oxide fouling curve, Re = 14000, 1500 ppm.

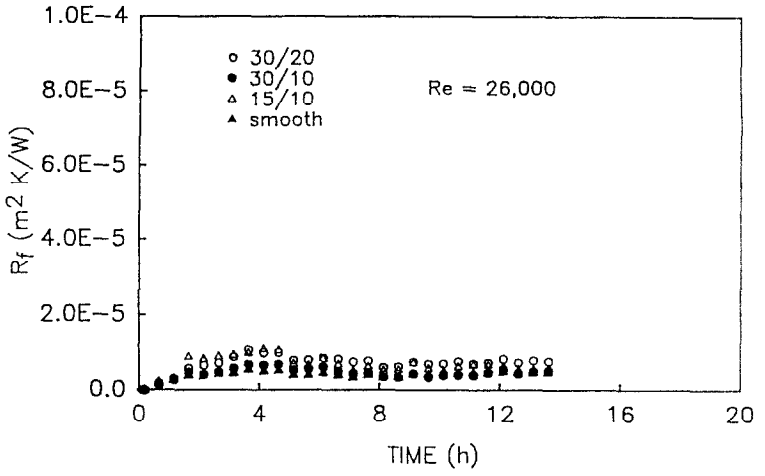

FIG. 11. Aluminum oxide fouling curve, $Re = 26000$, 1500 ppm.

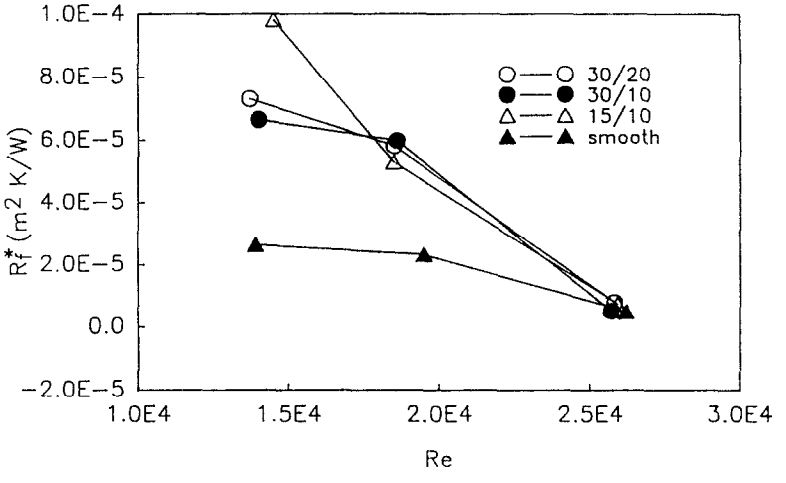

FIG. 12. Asymptotic fouling resistance vs Reynolds number, aluminum oxide, 1500 ppm.

Table 6. Table of exponents

Variables	R_f^*		$\dot{R}_{f0}$		S_{rep}/S_{sm}		ξ	
	F.O.	A.O.	F.O.	A.O.	F.O.	A.O.	F.O.	A.O.
e/D	−0.5	−0.3	−0.3	−0.3	−0.3	−0.2	−0.5	−0.7
p/e	0.1	0.3	0.4	0.2	0.6	0.3	0.1	0.2
Re	−3.8	−3.9	−1.5	−1.5	−2.2	−2.2		

In the table, the sticking probabilities are presented relative to those of the smooth tube. This was necessary to avoid the evaluation of the deposit density and the deposit thermal conductivity. S_{sm} is defined as the value obtained for the smooth tube at $Re = 14000$. Listed below are the observations of the functional dependencies.

(1) R_f^* shows very strong Reynolds number dependency compared with that of the smooth tube. The smooth tube Reynolds number dependency was −1.6 for ferric oxide fouling [16]. Table 6 also shows that R_f^* increases as e/D decreases and p/e increases.

(2) Table 6 shows that the sticking probability is approximately inversely proportional to the square of the Reynolds number. The sticking probability may be explained through the particle adhesion forces. The hydrodynamic lift force acting on the particle is proportional to the wall shear stress (equation (15)). The wall shear stresses between the ribs were calculated using the current model, and they were approximately proportional to the Reynolds number squared. If the hydrodynamic force controls the particle adhesion, then, $S \propto Re^{-2}$. This is in good agreement with the results in Table 6. Table 6 also shows that the sticking probability increases as p/e increases

Table 7. Comparison of the results with the previous models

Model	R_f^*	$\dot{R}_{f0}$	S
Kern–Seaton [21]	−1.1	0.8	
Watkinson–Epstein [22]	−3.0	−1.1	−2.0
Current results	−3.8	−1.5	−2.2

and e/D decreases. The predicted wall shear stress also shows the same tendency as shown in Fig. 8.

(3) Table 6 shows that the exponents for both foulants are approximately equal. The reason may be that the net forces acting on the particles are approximately the same for both foulants as shown in Table 2.

The current fouling results may be compared with the previous fouling models of Kern–Seaton [21] and Watkinson–Epstein [22]. The previous fouling models were originally developed to explain the fouling behavior in a smooth tube. Table 7 compares the Reynolds number exponents of the referenced models with the test results. The table shows that the current results reasonably match with the results of the Watkinson–Epstein model. This is expected because Watkinson–Epstein assumed that the sticking probability is inversely proportional to the wall shear stress, which they deduced from the consideration of the particle residence time at the wall. In this study, the velocity dependency of the sticking probability is derived based on the fundamental study of the forces acting on the particles.

In this study, discussions were limited to 1500 ppm concentration. Consideration of the forces acting on a particle at the wall, which was adopted to explain the trends of the sticking probability, does not seem to be affected by the amount of bulk concentration. If S and ξ are independent of the concentration, the current fouling model predicts that the fouling resistance is proportional to the concentration. However, the fouling results of commercial enhanced tubes [1] show only weak dependency on the concentration in the range between 750 and 2500 ppm, which implies that the sticking probability decreases with increasing concentration. Thus, it is recommended as a future work to investigate the effect of concentration both experimentally and theoretically.

4. CONCLUSIONS

A rationally based fouling model applicable to repeated rib tubes was developed. The model, with experimentally determined sticking probability and deposit bond strength factor, can predict the fouling behavior of repeated rib tubes. The mass transfer rate is assumed to control the particle transport process, and the wall shear stress is assumed to control the removal process. The mass transfer rate for the repeated rib tubes is obtained from the corresponding heat transfer correlations. The wall shear stress is modeled based on the flow structure between the ribs.

Particulate fouling tests were conducted. The variables investigated in this study are the roughness variables ($0.015 < e/D < 0.030$ and $10 < p/e < 20$), Reynolds number ($14\,000 < Re < 26\,000$) and the foulant material (ferric oxide and aluminum oxide). The tube material is copper, and the rib cross-section is arc-shaped. Listed below are the conclusions.

(1) Empirical correlations of the sticking probability and the deposit bond strength factor were determined. The exponents are given in Table 6.

(2) An analysis was performed that accounts for the forces acting on the particles at the wall. This analysis suggests that the hydrodynamic force controls the adhesion process in the present tests. The analysis qualitatively supports the functional dependency of the sticking probability.

(3) The fouling resistances of the repeated rib tubes were higher than those of the smooth tube at low Reynolds numbers. At a high Reynolds number ($=26\,000$), however, they were approximately the same as the smooth tube value. Within the test range, the fouling resistance increases as e/D decreases and p/e increases.

REFERENCES

1. R. L. Webb and N.-H. Kim, Particulate fouling of internally-ribbed tubes. In *Heat Transfer Equipment Fundamentals, Design, Applications and Operating Problems* (Edited by R. K. Shah), HTD-108, pp. 315–324. ASME (1989).
2. R. J. Patun, R. H. Krueger and K. Starner, Fouling studies and heat transfer test stand real time data acquisition system. In *Fouling of Heat Transfer Equipment* (Edited by E. F. C. Sommerscales and J. G. Knudsen), pp. 111–131. Hemisphere, Washington, DC (1981).
3. A. P. Watkinson, L. Louis and R. Brent, Scaling of enhanced heat exchanger tubes, *Can. J. Chem. Engng* **52,** 558–562 (1974).
4. G. A. Dreytser, V. I. Gomon and I. Z. Aronov, Comparison of fouling in tubes with annular turbulence promoters and in tubes of smooth shell-and-tube heat exchangers, *Heat Transfer—Sov. Res.* **15**(1), 87–93 (1983).
5. J. G. Knudsen and H. K. McCluer, Hard water scaling of finned tubes at moderate temperatures, *Chemical Progress Symposium Series, Heat Transfer—Chicago*, Vol. 55, No. 29, pp. 1–4 (1959).
6. C. R. Bemrose and T. R. Bott, Correlations for gas-side fouling of finned tubes, *The Institution of Chemical Engineers Symposium Series No. 86, First U.K. National Conference on Heat Transfer*, pp. 357–367 (1984).
7. P. Sheikholeslami and A. P. Watkinson, Scaling of plain and externally finned heat exchanger tubes, *J. Heat Transfer* **108,** 147–152 (1986).
8. N. Epstein, Particulate fouling of heat transfer surfaces: mechanisms and models. In *Fouling Science and Technology* (Edited by L. F. Melo, T. R. Bott and C. A. Pinheiro), pp. 173–189. Kluwer Academic (1988).
9. P. G. Papavergos and A. B. Hedley, Particle deposition behavior from turbulent flows, *Chem. Engng Res. Des.* **62,** 275–295 (1984).
10. D. F. Dipprey and R. H. Sabersky, Heat and momentum transfer in smooth and rough tubes, *Int. J. Heat Mass Transfer* **6,** 329–353 (1963).
11. L. A. Hahn, J. J. Stukel, K. H. Leong and P. K. Hopke, Turbulent deposition of submicron particles on rough walls, *J. Aerosol Sci.* **16**(1), 81–86 (1985).

12. B. A. Kader and A. M. Yaglom, Turbulent heat and mass transfer from a wall with parallel roughness ridges, *Int. J. Heat Mass Transfer* **20,** 345–357 (1977).
13. R. L. Webb, E. R. G. Eckert and R. G. Goldstein, Generalized heat transfer and friction correlations for tubes with repeated-rib roughness, *Int. J. Heat Mass Transfer* **15,** 180–184 (1971).
14. H. C. Lavallee and A. T. Popovich, Fluid flow near roughness elements investigated by photolysis method, *Chem. Engng Sci.* **29,** 49–59 (1974).
15. M. J. Lewis, An elementary analysis for predicting the momentum and heat transfer characteristics of a hydraulically rough surface, *ASME J. Heat Transfer* **97**(2), 249–254 (1975).
16. N.-H. Kim, A theoretical and experimental study on the particulate fouling of tubes having two-dimensional roughness, Ph.D. Thesis, The Pennsylvania State University, University Park, Pennsylvania (1989).
17. J. Visser, Adhesion and removal of particles—part 1. In *Fouling Science and Technology* (Edited by L. F. Melo, T. R. Bott and C. A. Piheiro), pp. 87–104. Kluwer Academic (1988).
18. L. F. Melo and C. A. Pinheiro, Fouling by aqueous suspension of kaoline and magnetite: hydrodynamic and surface phenomena effects. In *Fouling Science and Technology* (Edited by L. F. Melo, T. R. Bott and C. A. Pinheiro), pp. 173–189. Kluwer Academic (1988).
19. M. A. Hubbe, Theory of detachment of colloidal particles from flat surfaces exposed to flow, *Colloids Surfaces* **12,** 151–178 (1984).
20. N.-H. Kim and R. L. Welch, Particulate fouling in tubes having arc-shaped two-dimensional roughness by a flowing suspension of aluminum oxide in water, *Heat Transfer 1990, Proc. 9th Int. Heat Transfer Conf.*, Vol. 5, pp. 139–144 (1990).
21. D. Q. Kern and R. E. Seaton, A theoretical analysis of thermal surface fouling, *Br. Chem. Engng* **14**(3), 258–262 (1959).
22. A. P. Watkinson and N. Epstein, Particulate fouling of sensible heat exchangers, *4th Int. Heat Transfer Conf.*, Versailles, Vol. 1, Paper HE 1.6 (1970).

ENCRASSEMENT PARTICULAIRE D'EAU DANS LES TUBES AYANT UNE RUGOSITE A GEOMETRIE BIDIMENSIONNELLE

Résumé—On développe un modèle d'encrassement établi rationnellement. Le modèle peut prédire l'encrassement de tubes avec des nervures répétées. Le flux de masse transféré est supposé contrôler le mécanisme de transfert des particules et le frottement pariétal est supposé contrôler le mécanisme d'enlèvement. Ce flux est obtenu à partir des corrélations de transfert de chaleur. La contrainte de frottement pariétal est basée sur la structure de l'écoulement entre les rainures. Des tests d'encrassement particulaire sont conduits dans l'eau. Les paramètres sont les variables de rugosité ($0{,}015 \leqslant e/D \leqslant 0{,}030$ et $10 \leqslant p/e \leqslant 20$), le nombre de Reynolds ($14\,000 \leqslant Re \leqslant 26\,000$) et le matériau d'encrassement (oxyde de fer et oxyde d'aluminium). Le matériau du tube est le cuivre et les nervures ont des profils en forme d'arc. Des formules empiriques donnent l'effet des paramètres géométriques et d'écoulement. Une analyse prend en compte les forces qui agissent sur les particules à la paroi. Elle suggère que la force hydrodynamique est dominante pour les tests effectués. Elle conforte les dépendances obtenues empiriquement de la probabilité de dépôt vis-à-vis du nombre de Reynolds.

SCHMUTZABLAGERUNG IN WASSERDURCHSTRÖMTEN ROHREN MIT ZWEIDIMENSIONALER RAUHIGKEIT

Zusammenfassung—In der vorliegenden Arbeit wird ein rational begründetes Verschmutzungsmodell angreifenden Kräfte werden berechnet. Dabei zeigt sich, daß bei den durchgeführten Versuchen die Ablagerung eingeführt, was die Vorausberechnung des Verschmutzungsverhaltens von Rohren mit regelmäßiger Berippung erlaubt. Es wird angenommen, daß der Stofftransport den Vorgang des Partikeltransportes bestimmt, während die Wandschubspannung den Ablöseprozeß beeinflußt. Der Stofftransport in den betrachteten berippten Rohren wird aus entsprechenden Wärmeübergangskorrelationen ermittelt. Die Wandschubspannung ergibt sich aufgrund der Strömungsstruktur zwischen den Rippen. Versuche zur Schmutzablagerung werden in Wasser ausgeführt, wobei der Einfluß folgender Größen untersucht wird: die Rauhigkeitsvariablen ($0{,}015 \leqslant e/D \leqslant 0{,}030$ und $10 \leqslant p/e \leqslant 20$), Reynolds-Zahl ($14\,000 \leqslant Re \leqslant 26\,000$) und verschmutzende Substanz (Eisenoxid und Aluminiumoxid). Das Rohr besteht aus Kupfer, der Rippenquerschnitt ist bogenförmig. Empirische Korrelationen beschreiben den Einfluß der Geometrie- und Strömungsparameter auf die Haftwahrscheinlichkeit und den Haftkraftfaktor. Die an den Partikeln angreifenden Kräfte werden berechnet. Dabei zeigt sich, daß bei den durchgeführten Versuchen die hydrodynamische Kraft bestimmend ist. Die Untersuchung bestätigt die empirisch ermittelte Abhängigkeit der Haftwahrscheinlichkeit von der Geometrie und von der Reynolds-Zahl.

ХАОТИЧЕСКОЕ ОСАЖДЕНИЕ ЧАСТИЦ ИЗ ВОДЫ В ТРУБХ С ДВУМЕРНОЙ ШЕРОХОВАТОСТЬЮ

Аннотация—Разработана модель столкновения частиц, которая при наличии экспериментальных данных по вероятности прилипания и коэффициенту прочности сцепления осадка может использоваться для определения хаотического осаждения в периодически оребренных трубах. Предполагается, что скорость массопереноса управляет процессом переноса частиц, в то время как напряжение сдвига определяет процесс удаления. Из соответствующих соотношений для теплопереноса найдена скорость массопереноса в случае периодически оребренных труб. Напряжение сдвига на стенке моделируется на основе структуры труб. Напряжение сдвига на стенке моделируется на основе структуры течения между ребрами. Эксперименты по хаотическому осаждению частиц проводились в воде. В данной работе использовались трубы с различной шероховатостью, число Рейнольдса изменялось в пределах $14\,000 \leq Re \leq 26\,000$, в кауестве материала применялись окись железа и окись алюминия. Труба была изготовлена из меди, а поперечное сечение ребра имело аркообразную форму. Эмпирические соотношения определяют влияние геометрических параметров и характеристик течения на вероятность прилипания и коэффициент прочности сцепления. Проведен анализ сил, воздействующих на частицы у стенки, который позволил сделать предположение, что в настоящих экспериментах доминирует гидродинамическая сила. Анализ качественно подтверждает эмпирически полученные зависимости вероятности прилипания от геометрии и числа Рейнольдса.